



Sandwich-Type Composites Based on Smart Ionomeric Polymer and Electrospun Microfibers

Valentina Sessini¹, Antonio Julio López Galisteo², Adrián Leonés¹, Alejandro Ureña² and Laura Peponi^{1*}

¹ Institute of Polymer Science and Technology (ICTP), Spanish National Research Council, Madrid, Spain, ² Departamento de Matemática Aplicada, Ciencia e Ingeniería de Materiales y Tecnología Electrónica, Escuela Superior de Ciencias Experimentales y Tecnología, Universidad Rey Juan Carlos, Móstoles, España

OPEN ACCESS

Edited by:

Alfonso Maffezzoli,
University of Salento, Italy

Reviewed by:

Carola Esposito Corcione,
University of Salento, Italy
Silvia E. Barbosa,
CONICET Planta Piloto de Ingeniería
Química (PLAPIQUI), Argentina

*Correspondence:

Laura Peponi
lpeponi@ictp.csic.es

Specialty section:

This article was submitted to
Polymeric and Composite Materials,
a section of the journal
Frontiers in Materials

Received: 30 July 2019

Accepted: 08 November 2019

Published: 03 December 2019

Citation:

Sessini V, López Galisteo AJ,
Leonés A, Ureña A and Peponi L
(2019) Sandwich-Type Composites
Based on Smart Ionomeric Polymer
and Electrospun Microfibers.
Front. Mater. 6:301.
doi: 10.3389/fmats.2019.00301

Taking advance of the fiber-reinforced polymer process, commonly used in the fabrication of polymer composites, in this work we used electrospun microfibers to reinforce self-healing ionomeric polymers producing sandwich-type composites. In particular, three-layer stack with poly(lactic acid), PLA, electrospun fibers in between two layers of commercial smart polymers has been obtained based on poly(ethylene-co-methacrylic acid) (EMAA) copolymers, well-know with the tradename of Nucrel[®] and Surlyn[®], both of them manufactured by DupontTM Company. Surlyn[®] is the corresponding ionomer of Nucrel[®] in which the MAA groups are partially neutralized with sodium ions. In general, one of the main problems of thermoplastic composites, that provoke a lower impregnation of the fiber, is the high viscosity of the molten matrix. Therefore, in this work, we used electrospun microfibers in order to solve impregnation problem, thus considering that electrospinning process is an accessible, versatile and low-cost technique for fibers formation in the range of micron and nanometers. In order to create the sandwich-type structure, firstly, the optimization of the processing window has achieved in order to maintain the randomly oriented fiber structure on the final composites. In particular, the creation of sandwich-type structure with Surlyn[®] reinforced with woven non-woven electrospun fibers based on PLA with enhanced mechanical as well as hardness and wear resistance can be used for future active packaging solutions.

Keywords: sandwich, electrospun microfibers, PLA, ionomers, EMMA copolymers, polymer composite

INTRODUCTION

From the beginning, polymeric composite materials play a very important rule in the field of engineering materials. In general, with the term composite material we refer to a material prepared starting from two or more components with significantly different physical or chemical properties that, when combined, produce a material with characteristics completely different from the individual ones (Kar, 2016; Sessini et al., 2019). Thermosetting as well as thermoplastic polymers can be used in order to obtain polymer composite materials (Salomi et al., 2007; Zhu et al., 2011). Their applications are disparate covering all the fields that surround us, from aeronautics to construction, from biomedicine to daily-use objects, among others (Wang et al., 2017). Nowadays particular importance is also focused on nanocomposites materials, where at least one component has to show dimension in the nano range (Peponi et al., 2014).

Different and many are the techniques used to obtain polymeric composite materials such as compression molding, autoclave and vacuum bag, preforming, filament winding, pultrusion, resin transfer molding and so on, depending on the thermo-response of the polymeric matrix used (Kim and Lee, 2016).

Another important process used when working with polymer composites is the fiber-reinforced polymer (FRP) commonly used in aerospace, automotive, construction, marine and ballistic field (Ku et al., 2011; Pickering et al., 2016). In this case, glass fibers as well as carbon fibers are generally used and the process can be divided in two main part, (i) the fibers fabrication and (ii) the molding process used to bond the fibers with the polymeric matrix. In general, one of the main problems of thermoplastic composites, that provoke a lower impregnation of the fiber, is the high viscosity of the molten matrix. In order to solve the problem, many manufacturing processes for thermoplastic composites have been developed and in particular, the use of a prepreg is commonly preferred in industrial practice (Dell'Anna et al., 2018).

Taking advance of the FRP process, commonly used in the fabrication of polymer composites, in this study we used electrospun microfibers to reinforce self-healing ionic polymers creating sandwich-type structures, in order to solve the impregnation problem of the fibers.

The idea of using fibers obtained by electrospinning is based on the increasing development of electrospinning technique in the last years as well as on the characteristics own of the electrospun fibers that is both high surface-to-volume and large length-to-diameter ratios (Fang et al., 2008; Persano et al., 2013).

Electrospinning process is an accessible, versatile and low-cost technique for fibers formation in the range of micron, and nanometers. This technique usually consists in a syringe containing the polymeric solution which flows through the needle connected to an electrode. The other electrode is connected to the collector and when a voltage is applied, the electrostatic force stronger than gravity force transforms the solution drop in a cone, named "Taylor cone" from which fibers are ejected (Amiraliyan et al., 2009). The distance between the needle and the collector has to be enough to permit the evaporation of solvent and the fibers are randomly collected in woven non-woven fiber mats. Apparently simple, this technique required the optimization of different parameters, such as those related to the polymeric solution like the solution concentration, solvent type, superficial tension of solutions, those relate with the electrospinning itself as applied voltage, solution flow rate, distance between the needle and the collector, and also ambient parameters such as temperature and humidity conditions, to control uniformity on geometry and diameter of the fibers (Carrasco-Hernandez et al., 2017).

Additionally, due to the very high surface-to-volume ratio typical of electrospun fibers, the interaction with a matrix, is expected to be significantly enhanced, leading to a high strengthening efficiency. For these reasons, electrospun mats have been recently proposed as reinforcement of polymers as a good alternative to conventional reinforcing fibers (Li and Xia, 2004). Moreover, electrospun fibers can be used

to incorporate nanoscale fillers and/or plasticizer to enhance mechanical properties as well as to give a multi-functionality and multi-response behavior to the electrospun fibers (Sonseca et al., 2012; Peponi et al., 2014; Arrieta et al., 2016a,b; Leonés et al., 2019).

The use of electrospun fibers to reinforce polymer composite materials is quite new thus considering that very few scientific articles, about 10 from Scopus source, were published up to now and most of them were published on 2019.

Lamastra et al. (2012) published for the first time in 2012 a study to fabricate nanocomposites with electrospun fibers as reinforcing element. In particular, they used polycaprolactone, PCL, as matrix and electrospun fibers of polymethylmethacrylate, PMMA reinforced with both multiwall carbon nanotubes (MWCNT) and graphene nanoplatelets (GNP). They fabricated the composite by using 5 layers of the matrix and 4 layers of the electrospun fiber reinforcements alternatively stacked. They found that all composites show a strong interface necessary for an efficient load transfer from the matrix to the electrospun fiber reinforcement.

In Kim et al. (2013) studied composites based on electrospun SiC fibers and phenolic resin for application as high thermal conducting substrate for the fabrication of heat dissipating microelectronic components. In particular, they synthesized silicon carbide from the pyrolysis of cured polycarbosilane fibers and obtained that for 40 wt% SiC content the thermal conductivity strongly increases.

In Cherpinski et al. (2018) reported a work on multilayer structures based on annealed electrospun biopolymer of interest in water and aroma barrier for food packaging applications, in particular for fiber-based packaging.

In Cai et al. (2019) studied the effect of electrospun polysulfone/cellulose nanocrystals interleaves on the interlaminar fracture toughness of carbon fiber/epoxy composites.

The use of electrospun nanofibers loaded with active compounds as layer in composites materials is starting to focus the attention of scientist in last years. Arrieta et al. (2019) studied the antioxidant effect on biodegradable bilayers based on PHBV and plasticized electrospun fibers obtained by encapsulating catechin in the electrospun fibers as antioxidant carrier for food packaging application. Quiles-Carrillo et al. (2019) use electrospun fiber to produce PLA-based films multilayer with controlled release of garlic acid as antioxidant agent.

López-Córdoba et al. (2019) added electrospun PVA fibers to a starch matrix for active food packaging. Their cross-sections images revealed a sandwich-type structure, indicating that the electrospun mat was fully incorporated into the composites. In particular, the presence of the electrospun PVA mats provoked a significant reduction in the water vapor permeability of the film.

Moreover, Kimna et al. (2019) reported the fabrication of multilayer wound dressing membranes with controlled release of gentamicin to prevent the possible infections at the injured site.

Electrospun mats also showed high porosity and excellent flexibility so can be added in composites to achieve new small sized and weight light devices. Some examples of these kinds of materials can be found in the literature. For example,

Khalid et al. (2019) fabricated a highly sensitive biodegradable pressure sensor based on nanofibrous dielectric to be used in biomedical implants or short-term communication devices based on electrospun PLGA-PCL membranes. Moreover, Oroujzadeh et al. (2019) studied electrospun fibers of non-sulfonated poly(ether ketone) PEK obtained by electrospinning and the fibers were impregnated with 70% sulfonated polymer solution to make blend membranes with controlled water absorption and increased mechanical strength.

Therefore, electrospun fibers characteristics provide a wide range of advantages in the fabrication of composite materials whose applicability is being studied in different fields such as the fabrication of epoxy composite (Cai et al., 2019) fabrication of resin (Kim et al., 2013) or water and aroma filters (Cherpinski et al., 2018) as well as packaging application (Arrieta et al., 2015). Among their different advantages, electrospun fibers are widely used as carriers for active compounds. The controlled release of chemicals provides for example, an efficient mechanism for preventing infections or for protecting food products from the contamination.

Consequently, based on these advances in the use of electrospun fibers, in this work we obtain PLA electrospun fibers to achieve a sandwich-type structure in between matrix of commercial smart polymers. In particular two different matrices have been used based on poly(ethylene-*co*-methacrylic acid) (EMAA) copolymer well-know with the tradename of Nucrel[®] and Surlyn[®] both of them manufactured by Dupont[™] Company.

In particular, Nucrel[®] is an EMAA copolymer used for foil adhesive and heat sealant coating (DiPoto, 1996; Krabbenborg et al., 2007). Surlyn[®] is its corresponding ionomer in which the MAA groups are partially neutralized with sodium ions and it is used as material for innovative packaging in photovoltaic applications (Lertngim et al., 2017), traditional packaging from cosmetic to food (Varley, 2007) and for golf ball encapsulation (Varley, 2007). Surlyn[®] is able to present both shape memory and self-healing behavior (Varley et al., 2010; Lu and Li, 2016). Sessini et al. (2018) studied the shape memory response of nanocomposites based on both Nucrel[®] and Surlyn[®] reinforced with different amount of silica nanoparticles.

Lu and Li (2016) reported that commercial Surlyn[®] 8940, neutralized with sodium, exhibits both one-way multi-shape memory effects and tunable two-way reversible actuation. Zhao et al. (2017) demonstrated shape memory behavior of 3D printed objects using the same commercially available zinc neutralized EMAA without any modification. Calderón-Villajos et al. (2019) also demonstrate that 3D-printing Surlyn[®] based nanocomposites, reinforced with multiwall carbon nanotubes, show increasing mechanical response maintaining its self-healing properties.

The self-healing properties of this polymer under high speed impact (Varley and van der Zwaag, 2008; Varley et al., 2010), and even under hyper-velocity impacts simulating space debris impacts (Francesconi et al., 2013) has been also studied.

Thermal response of this thermoplastic copolymer was studied by Kalista and Ward (2007) to better understand the self-healing capabilities and the mechanism taking place in the

material not only at room temperature, but even under low temperature damaging of the polymer.

Scratch healing behavior of this ionomer and the influence of free carboxylic groups was evaluated by Vega et al. (2014). This scratch resistance is vital in packaging and encapsulating applications of the ionomer.

Sundaresan et al. (2013) studied the self-healing properties of composites based on woven carbon fibers embedded on Surlyn[®] indicating that the composite can sustain damage from medium-velocity impact and heal from the energy of the impact.

Therefore, in this work, woven non-woven PLA electrospun fibers randomly oriented are arranged in between two layers of Nucrel[®] and Surlyn[®] sheets (0.500 mm thick) and melt-pressed into an innovative composite. Particular care has been taken on the processing window to obtain the final composite. In particular, the creation of sandwich-type structure with Surlyn[®] reinforced with woven non-woven electrospun fibers based on PLA with enhance mechanical as well as hardness and wear resistance can be used for potential innovative packaging, from cosmetic, food and photovoltaic applications.

MATERIALS AND METHODS

Materials

Commercial poly(ethylen-*co*-methacrylic acid) random copolymer named Nucrel[®] 960 [contained 15 wt.% of methacrylic acid (MAA) comonomer] and its ionomer, Surlyn[®] 8940, with 30% of MAA comonomer neutralized by sodium, were kindly provided by Dupont[™] Company. Nucrel[®] 960 and Surlyn[®] 8940 referred to as “Nucrel” and “Surlyn” respectively, from this point forward.

Poly(lactic acid) (PLA2003D, molecular weight 12×10^4 g/mol, 4.25% of D-lactic acid monomer) was supplied by Nature Works[®].

Chloroform (CHCl₃) from Sigma Aldrich was used as solvent.

Production of Microfiber by Electrospinning

PLA pellets were dried in oven overnight at 60°C before use. PLA solution with a concentration of 10 wt% in CHCl₃ was stirred overnight at room temperature before the electrospinning process as indicating in our previous work (Mujica-Garcia et al., 2014).

The polymer solution of PLA was pumped through the inner needle and chloroform as solvent was pumped through the outer needle.

A voltage of 10.5 kV was applied in positive pole and -10.5 kV in negative pole producing the electric field. The solvent solution and polymer solution flow rates were fixed at 0.30 and 0.3 mL/h, respectively. This formulation was electrospun for 4 h over a metal plane collector covered with aluminum foil placed at 17.5 cm distance from the needle, obtaining a woven non-woven electrospun mat with thickness of 0.5 μm. The obtained mats were vacuum dried for 24 h in order to remove any solvent residues.

Fabrication of Sandwich-Type Composites

Before their processing, the polymers and the electrospun microfibers, named ePLA, were dried at 60°C for 48 h.

The composite sandwich-type structures were processed following two steps.

In the first one the films based on Nucrel and Surlyn of 0.5 mm were processed by compression molding of the pellets in a Dr. Collin 200 × 200 mm press at 160°C applying 50 bars of pressure for 3 and 2 min with water circulation to cool down the temperature. This procedure was used to produce the unreinforced polymer films.

In the second step, the sandwich-type structure was prepared by placing the electrospun PLA microfiber mat in between two layer of Nucrel or Surlyn, as reported in the **Figure 1** and compressed, obtaining a three-layer stack of Nucrel/ePLA/Nucrel or Surlyn/ePLA/Surlin, named Nu/ePLA/Nu and Su/ePLA/Su, respectively.

The compression molding of the sandwich-type structure was performed using two different processing window in order to study how the processing conditions can influence the fibers structure into the sandwich-type structures and their impregnation as well as their adhesion within the polymeric layers of the final composites.

In particular, in the first case, the compression molding was performed at 160°C, 50 bars for 3 min and cooling down the temperature for 2 min by water circulation. In the second case, the parameters have been fixed at 120°C, 50 bars of pressure for 3 min and cooling down the temperature for 2 min by water circulation.

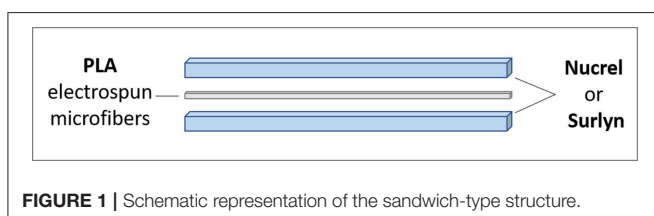
In order to compare the effect of the electrospun fiber addition procedure in the composite a bilayer of Nucrel/Nucrel (Nu/Nu) and Surlyn/Surlyn (Su/Su) have been also processed as reference samples.

Characterization Methods

The morphology of the sandwich-type composites was first studied by optical microscopy and by using of 3D Optical Profilometry (Zeta 20 from Zeta Instrument).

In order to better characterize the morphology at the interface between the different polymeric layers, SEM micrographs of the cryo-fracture surface of the Nucrel- and Surlyn-based composites, were obtained by scanning electron microscopy, SEM, PHILIPS XL30 with a tungsten filament. The sandwich-type composites were frozen using liquid nitrogen and then cryo-fractured. All the samples were gold/palladium coated by an automatic sputter coated Polaron SC7640.

SEM PHILIPS XL30 has been used also to characterize the PLA electrospun fibers, ePLA.



The thermal properties were investigated by Differential Scanning Calorimetry (DSC) analysis using a Mettler Toledo DSC822e instrument, under nitrogen flow (30 ml/min). Samples of about 10 mg were sealed in aluminum pans. The thermal analysis was programmed at 10°C min⁻¹ from 0°C up to 200°C obtaining the melting temperature (T_m) and the melting enthalpy (ΔH_m). Moreover, the degree of crystallinity (X_c) of each sample was calculated, according with the equation below:

$$\chi_c (\%) = \left(\frac{\Delta H_m}{\Delta H_m^{100}} \right) \times 100 \quad (1)$$

where, ΔH_m¹⁰⁰ is the specific melting enthalpy for a 100 % crystalline PE (278 J/g) (Weigel, 1981). The degree of crystallinity was calculated considering both melting peaks showed by the EMMA copolymers.

For the PLA electrospun fiber also a DSC scan has been obtained at the same experimental condition than the sandwich-type composite structures.

Thermogravimetric analysis (TGA) was carried out using a TGA Q500 thermal analyzer from TA Instrument. All samples were analyzed by dynamic mode using about 10 milligrams of sample from room temperature to 800°C at 10°C min⁻¹ under nitrogen atmosphere with a flow of 60 mL min⁻¹. Temperatures at the maximum degradation rate (T_{max}) were calculated from the first derivative of the TGA curves (DTG).

Dynamic Mechanical Thermal Analysis (DMTA) of the samples was carried out using a DMA Q800 from TA Instrument in film tension mode with an amplitude of 5 μm, a frequency of 1 Hz, a force track of 125 %, and a heating rate of 2°C min⁻¹. Samples subjected to DMA were cut from compression-molded films into regular specimens of approximately 20 mm × 5 mm × 0.90 mm.

Mechanical properties were determined using an Instron Universal Testing Machine at a strain rate of 150 mm min⁻¹. Tensile test measurements were performed on 5 dog-bone specimens with a width of 2 mm, thickness of 0.90 mm and leaving an initial length between the clamps of 20 mm. From these experiments were obtained the elastic modulus, as the slope of the curve between 0 and 2 % of deformation, the elongation at break and the tensile strength.

Hardness tests using Shore D standard ASTM D2240-05 (ASTM, 2015) were conducted on the surface of the specimens, using a maximum load of 10 kg applied during 10 s on the surface of each samples. At least 10 measurements were conducted on each sample in order to have representative mean values.

Wear tests were carried out at room temperature and under dry sliding condition with a pin-on-disc configuration (Microtest tribometre) using the polymer specimens as the discs, with a size in mm of 4 × 4 × 3 mm. The counterbody was a carbon steel ball of 6 mm of diameter. The wear tests were carried out at room temperature in dry conditions under a load of 10 N and using 200 rpm as rotational speed of the specimens. The test was maintained until wear depth a total sliding distance of 1,000 m. The wear testing machine recorded

continuously the friction coefficient and the wear depth over the specimens.

3D Optical Profilometry was also used to study the wear mechanism of the materials and to calculate the lost volume of the worn track of each sample after the wear test. Big areas of the sample can be analyzed in 2D and 3D mode due to the ability of the equipment to electronically move the sample holder platform, take individual micrograph and rebuild the whole scanned area. Mountain Map software was used to create 3D micrographs from the data obtained from the 3D Optical Profilometer.

Volume loss during the wear tests was determined from the volume of the worn track. This volume was calculated during the test using the 3D micrographs obtained from the

3D optical Profiles and the subsequent treatment with Mountain Map software. To evaluate the wear mechanism of the material under different conditions, the Archard's law was applied (Archard, 1953):

$$\frac{V}{L} = K \frac{W}{H} = k_v W \quad (2)$$

where, V is the wear volume, L is the sliding distance, being the coefficient V/L the wear rate, W is the applied load, H is the hardness of the sample, K is the Archard's constant and k_v is the specific wear rate calculated from volume lost.

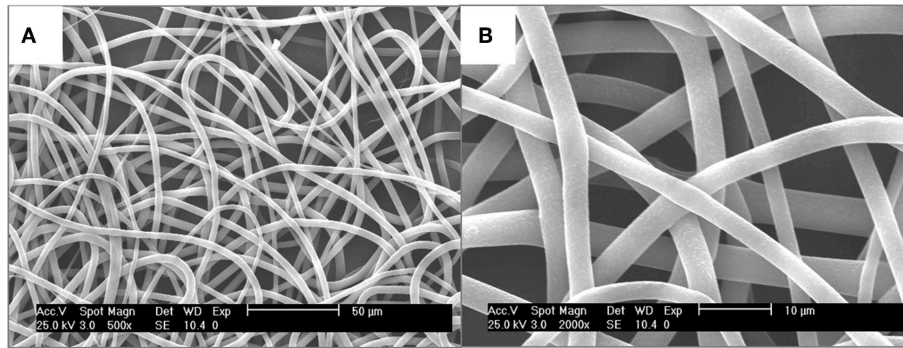


FIGURE 2 | (A,B) SEM images of PLA electrospun microfibers with different magnitudes.

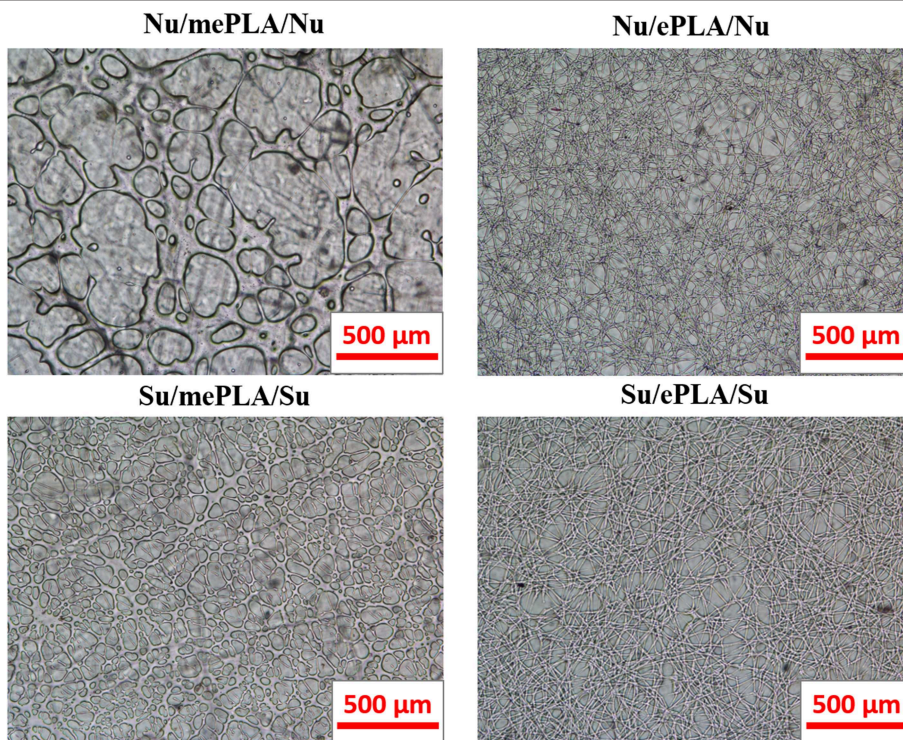


FIGURE 3 | OM images of Nucrel- and Surllyn-based multilayer composites reinforced with PLA electrospun microfibers.

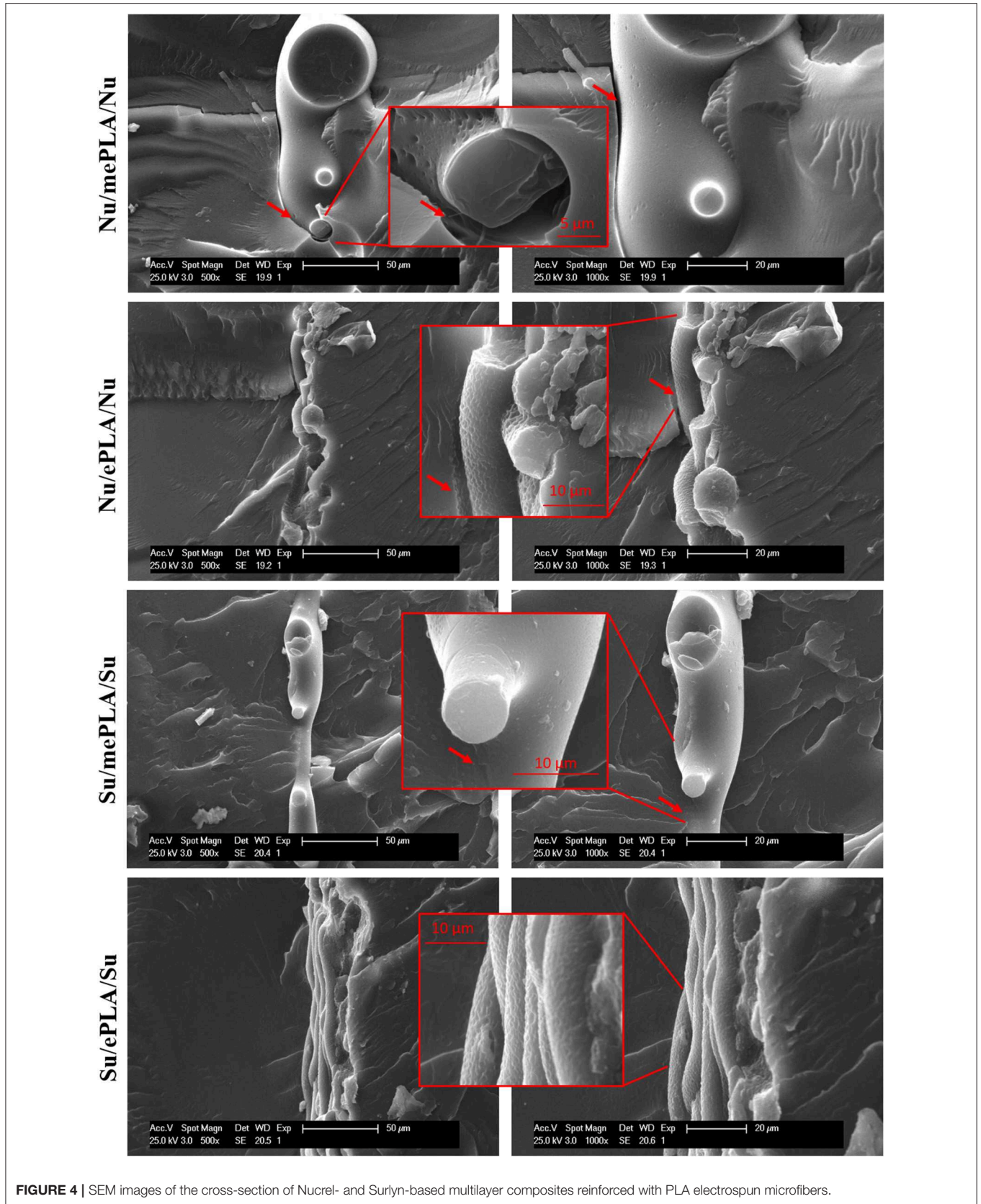


FIGURE 4 | SEM images of the cross-section of Nucrel- and Surllyn-based multilayer composites reinforced with PLA electrospun microfibers.

RESULTS AND DISCUSSION

Typically, carbon fiber structural composite materials are manufactured using layers of a woven fabric containing a few thousand reinforcing fibers stacked in different angular orientations (Barile and Casavola, 2019). In our case, randomly oriented woven non-woven PLA electrospun fiber mats are used in a three-layer stack of Nu/ePLA/Nu or Su/ePLA/Su.

First of all, once obtained the electrospun mats, their fiber morphologies were studied by scanning electron microscopy. SEM images of PLA electrospun microfibers are shown in **Figure 2**. As it can be seen, straight, randomly oriented and bead-free fibers were obtained with an average diameter of about $3.5 \pm 0.7 \mu\text{m}$.

On the other hands, the morphology of the sandwich-type composites obtained with the different temperature processing was firstly studied by OM and the OM micrographs are reported in **Figure 3**.

It is important to note that for the three-layer stack processed at 160°C the fibers lost their shape and are completely melted, in both Nucrel- and Surlyn-based multilayer composites. In this case, when the PLA electrospun fibers are completely melted, the samples are named Nu/mePLA/Nu and Su/mePLA/Su.

In the case of processing temperature of 120°C , non-melted fibers-based composites, have been obtained. This temperature ensures the adhesion between the polymeric layers of the sandwich structure but at the same time it is lower than the melting temperature of PLA maintaining the fiber structure. Therefore, it is clear to note, due to their transparency, that the final composites reinforced with not melted ePLA conserve the random oriented structure of the woven non-woven PLA electrospun fibers.

As it is possible to notice, there is a clear difference between the sample with melted and non-melted fibers. When the fibers are non-melted, their morphology is unmodified inside the sandwich structure while melted fibers-based samples show the coalescence of the fibers due to their melting, being this effect stronger in Nu/mePLA/Nu than the Surlyn-based sample, probably due to the elastomeric character of the Nucrel. However, in the case of non-melted fibers, the diameters of the PLA electrospun fibers incorporated in the sandwich structure change, enlarging

their values. In particular, for Nu/ePLA/Nu we obtained an average diameter of $7.3 \pm 1.9 \mu\text{m}$ while for Su/ePLA/Su an average value of $10.6 \pm 2.1 \mu\text{m}$ has been calculated based on 50 different measurements.

The morphology observed by OM was confirmed by SEM analysis. In **Figure 4**, the cryo-fractured surface micrographs of the three-layer stack composites are reported. The melting of the electrospun fibers is confirmed in both Nucrel- and Surlyn-based composites when the temperature of 160°C has been used during the manufacturing process. As it is easy to notice in **Figure 4** (inset), in the case of Nucrel-based composites an empty interface between the Nucrel matrix and the ePLA reinforcement is obtained. Completely different behavior was observed for Surlyn-based sandwich structures. This gap indicates low interaction between the PLA-based reinforcement and the Nucrel matrix, suggesting that the presence of the Na^+ ions in Surlyn-based composites increase the compatibility with PLA. Supporting this result, Jantanasakulwong et al. (2016) reported a similar result in 2016, for ternary blends based on PLA, acrylic rubber (ACM), and ethylene-methacrylic acid with sodium ions (EMAA-Na). They reported that the EMMA-Na can interact with both PLA and the ACM acting as compatibilizer between PLA and ACM. They demonstrated that the Na^+ ions in EMMA-Na were able to improve the interfacial adhesion through the end groups of PLA and the epoxy group of ACM because the Na^+ ion acted as a catalyst to accelerate the interfacial reaction.

TABLE 1 | Thermal properties of all the processed samples.

Sample	T_{m2} ($^\circ\text{C}$)	T_{m1} ($^\circ\text{C}$)	T_m PLA ($^\circ\text{C}$)	ΔH_m ($\text{J}\cdot\text{g}^{-1}$)	χ_c (%)	T_{max} PLA ($^\circ\text{C}$)	T_{max} ($^\circ\text{C}$)
Nu	45	93	–	36	12		461
Nu/Nu	45	92	–	50	17		467
Nu/mePLA/Nu	52	93	–	35	12	362	467
Nu/ePLA/Nu	45	93	148	63	22	368	472
Su	47	92	–	38	13		483
Su/Su	51	92	–	36	12		480
Su/mePLA/Su	45	92	–	33	11		480
Su/ePLA/Su	50	92	149	38	13		482

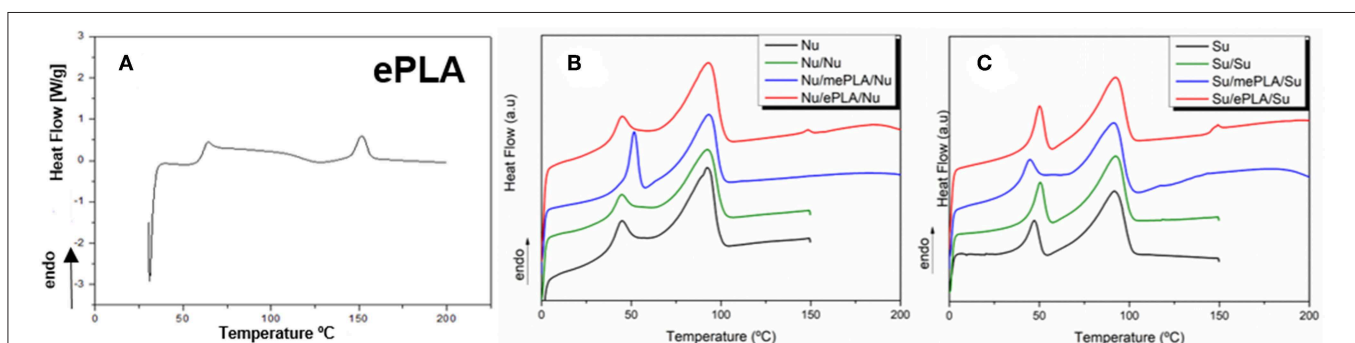


FIGURE 5 | First heating scan of DSC analyses for all the processed materials and their multilayer composites with PLA microfibers. **(A)** ePLA, **(B)** Nucrel-based multilayer composites, and **(C)** Surlyn-based multilayer composites.

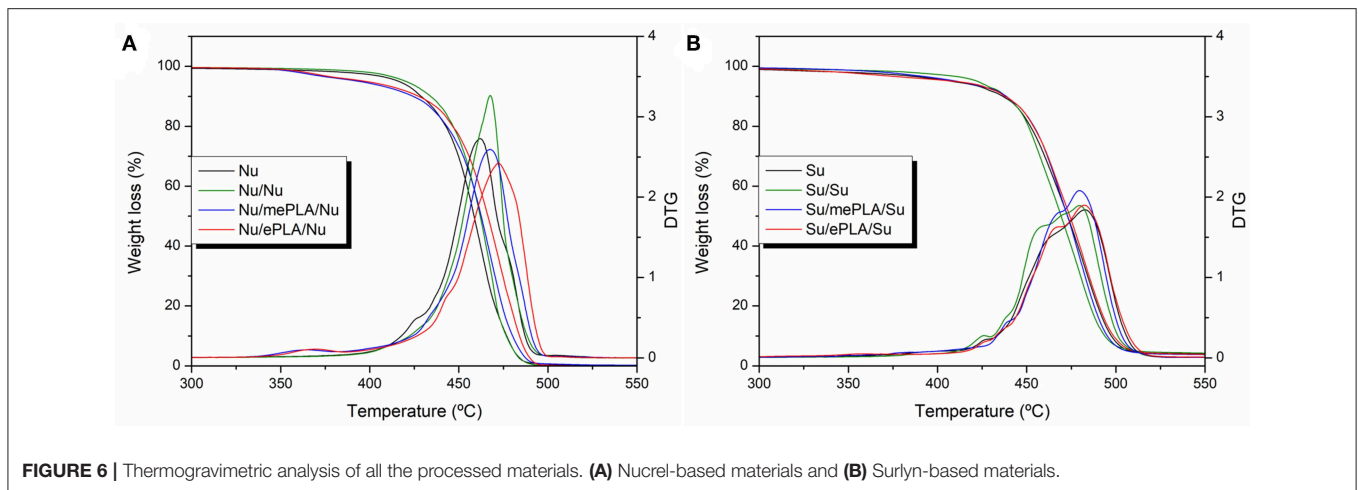


FIGURE 6 | Thermogravimetric analysis of all the processed materials. **(A)** Nucrel-based materials and **(B)** Surllyn-based materials.

The DSC thermograms for the electrospun fibers as well as for the sandwich structures are showed in **Figure 5**. In particular DSC thermogram for PLA electrospun fibers are reported in **Figure 5A**. Sandwich-type structure based on Nucrel[®] are reported in **Figure 5B** and the ones based on Surllyn[®] in **Figure 5C**. As it is possible to note, all the composite formulations exhibited the two characteristic endothermic peaks of EMAA-based materials. As reported in our previous work (Sessini et al., 2018), the highest temperature peak corresponds to the melting temperature of polyethylene crystals while the lowest temperature peak is ascribed to the melting of small polyethylene secondary crystals that slowly form following the primary crystallization (Marx and Cooper, 1974; Tsujita et al., 1987; Kuwabara and Horii, 2002; Loo et al., 2005; Dolog and Weiss, 2013). Moreover, the samples Nu/ePLA/Nu and Su/ePLA/Su showed an additional small endothermic peak at about 150°C, attributed to the melting of the semi-crystalline PLA electrospun microfibers impregnated inside to the sandwich structure. Moreover, thus comparing the sandwich structure obtained with the different processing temperature, it is easy to note the fiber structure is not modified when PLA melting temperature is not reached in the fabrication process.

The thermal properties of all the processed materials are summarized in **Table 1**. As it is possible to notice, an increase of the degree of crystallinity was observed for Nu/Nu probably due to the double processing that works as an annealing treatment for the sample. Furthermore, the presence of non-melted PLA microfiber in the sandwich structure of Nu/ePLA/Nu lead to the highest value of the degree of crystallinity. Nevertheless, no significant changes were observed in the degree of crystallinity value for Surllyn-based materials.

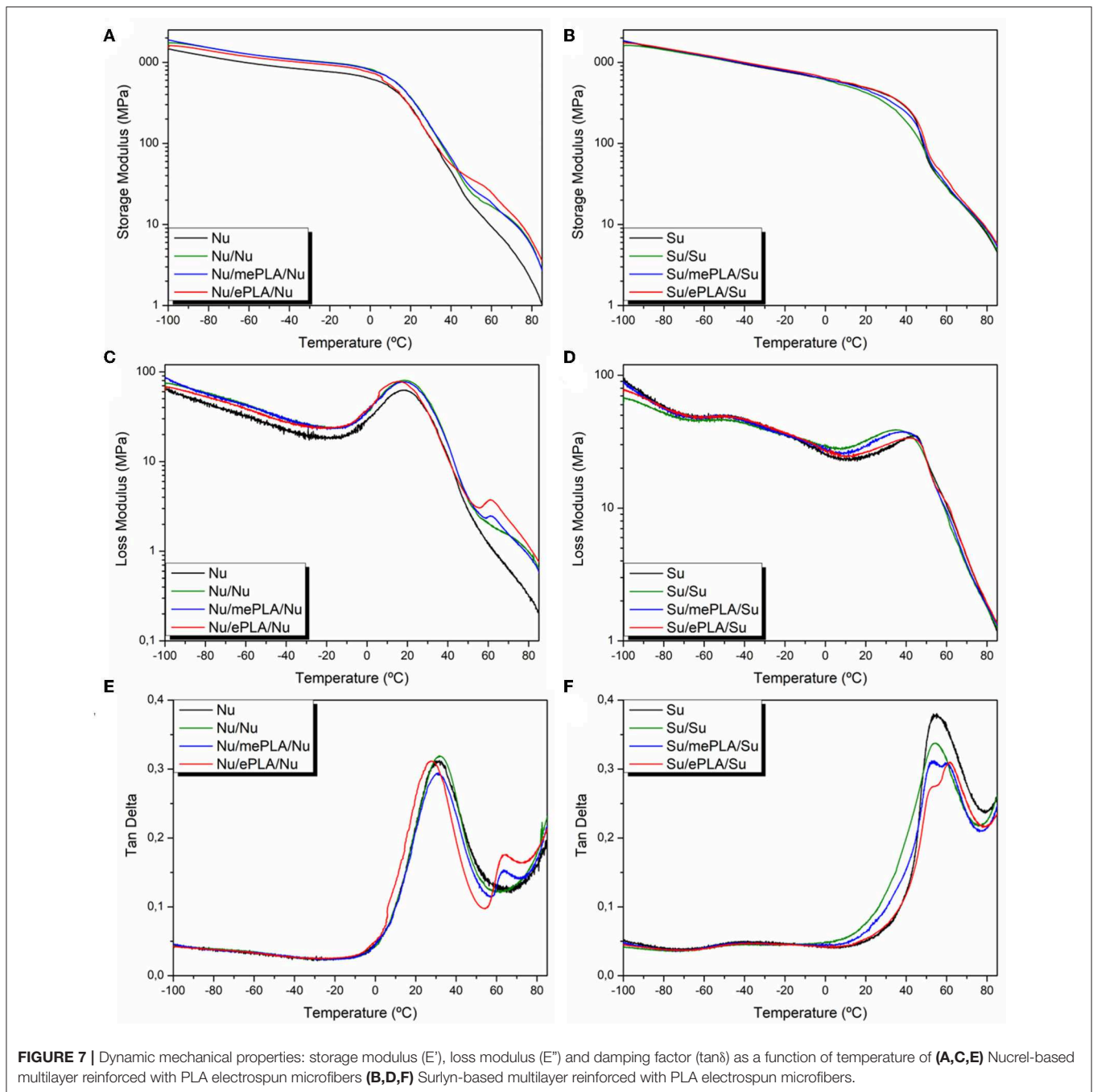
The TGA and DTG thermograms are reported in **Figure 6** for all the materials. Comparing the neat materials, Nucrel and Surllyn single films and bilayers, the presence of the neutralized MAA comonomer fraction with Na⁺ increases the thermal stability of the EMAA copolymers shift in the T_{max} of about 20°C, as reported previously (Sessini et al., 2018). Surprising, the presence of the PLA microfibers mat inside

the sandwich-type structure increased the thermal stability of Nucrel based materials of 6 and 11°C for Nu/mePLA/Nu and Nu/ePLA/Nu, respectively. Nevertheless, no significant changes in the thermal stability of Surllyn-based sandwich structure, due to the presence of PLA microfiber mat were observed. This behavior confirms the results previously obtained, Nucrel-based materials show less compatibility with PLA microfiber mat than Surllyn-based materials. This is due to the presence of the neutralized MAA comonomer fraction with Na⁺ in Surllyn-based materials, as previously reported in literature (Jantanasakulwong et al., 2016).

Dynamic thermo-mechanical analysis was performed in order to study the main chain relaxation in all EMAA-based materials and their composites. The storage modulus, loss modulus and $\tan\delta$ curves are reported in **Figure 7** for all the processed and fabricated materials. All EMAA-based materials have similar elastic properties. As reported in our previous work (Sessini et al., 2018), Nucrel-based materials showed three main relaxations. The first one is ascribed to a local molecular motion of the amorphous segment of PE (Tachino et al., 1993). The second one was assigned to a micro-Brownian segmental motion in the amorphous region (Eisenberg and Navratil, 1974; Tachino et al., 1993). While the third one was assigned to the melting of secondary crystals. However, for Surllyn-based materials, the same relaxations were observed but the peak corresponding to its T_{m2} is shifted to higher temperature compared with the Nucrel-based materials and a fourth relaxation was observed which was ascribed to the devitrification of ion-reach regions (Tachino et al., 1993). Furthermore, a latest peak was observed for both Nucrel- and Surllyn-based sandwich-type structure containing the melted and non-melted PLA microfiber mats which was ascribed to the T_g of PLA.

Figure 8 presents an example of the stress-strain curves obtained for all the processed materials.

Comparing Nucrel- and Surllyn-based materials, the neutralization of the MAA comonomer with Na⁺ provokes an increase of the mechanical properties showing higher elastic modulus and higher maximum stress values, as it was previously



reported (Sessini et al., 2018). The mechanical properties of all the processed materials are summarized in **Table 2**. As it is possible to notice, the elastic modulus of the reference samples increased more than three times for Nu/Nu and almost twice for Su/Su, probably due to the double processing treatment that in case of Nucrel increased also the degree of crystallinity, as it was observed in DSC analysis for Nucrel-based materials.

However, in the final part of this work, we prefer to focus the attention on the composite materials obtained with no-melted PLA electrospun fibers thus considering that, in case of melted

fibers we obtain a blend of two different materials rather than a sandwich-type structure.

Figure 9 shows a plain view micrograph of PLA reinforced Surllyn after its manufacturing process at 120°C. The 3D Optical Profiler used in this research has the ability to process 2D (**Figure 9A**) and 3D micrographs in which the different compositional planes of the transparent material are seen (**Figure 9B**). In 2D image the PLA electrospun fibers can be seen due to the optical transparency of Surllyn. In the 3D micrograph of **Figure 9B** the superior plane of Surllyn polymer can be seen

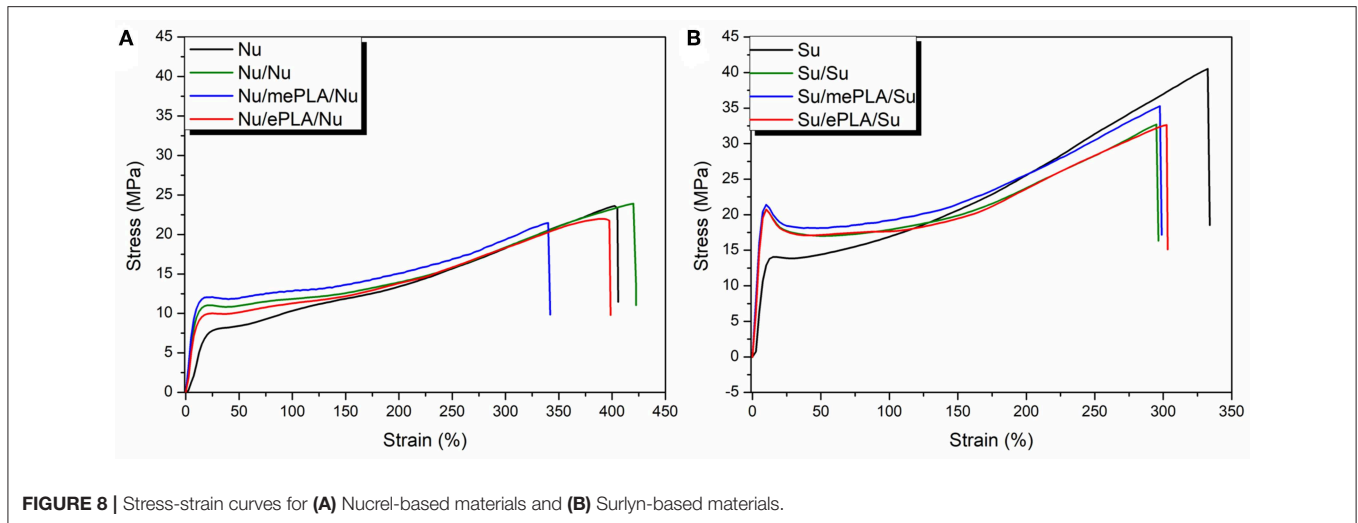


FIGURE 8 | Stress-strain curves for **(A)** Nucrel-based materials and **(B)** Surlyn-based materials.

TABLE 2 | Mechanical properties of the processed materials.

Sample	Elastic modulus (MPa)	Tensile strength (MPa)	Elongation at break (%)
Nu	32 ± 3	23.6 ± 0.2	405 ± 11
Nu/Nu	109 ± 3	23.5 ± 0.4	414 ± 15
Nu/mePLA/Nu	126 ± 17	21.5 ± 0.7	347 ± 13
Nu/ePLA/Nu	109 ± 10	22.1 ± 0.2	394 ± 14
Su	198 ± 8	41 ± 3	336 ± 28
Su/Su	307 ± 4	33 ± 2	294 ± 19
Su/mePLA/Su	318 ± 8	35 ± 2	297 ± 8
Su/ePLA/Su	305 ± 12	33.6 ± 0.9	325 ± 20

(with a scratch due to material manipulation) and also the inner plane of the material in which the PLA fibers are located, between the two plates of Surlyn can be seen. Post treatment of the digital micrograph allows to build up a 3D micrograph in which the higher Surlyn layer is delated and the PLA random mat can be observed in 3D. The individual PLA fibers are not melted because of the thermal treatment used to incorporate them in the final polymer matrix, as it was seen in the micrographs of **Figures 9A,C**.

Shore D hardness tests were conducted on the unreinforced and PLA reinforced composites (**Figure 10A**). Hardness values of unreinforced thermoplastics are quite similar, with values around 46. The addition of PLA in the polymer matrix increases around a 30 % the hardness of the material, with final values around 60. This higher hardness must lead to a better wear performance of both reinforced polymers.

In order to confirm this, wear tests at room temperature were carried out using the procedure and the configuration indicated in the experimental section. Coefficient of Friction (CoF) and the specific wear rate (k_v) was determined for the different tested specimens.

Nucrel, Surlyn and its PLA reinforced composites are plotted in **Figure 10B** in terms of CoF and sliding distance recorded

during the wear tests. CoF increases during the test in the case of unreinforced polymers and in the case of Nu/ePLA/Nu sample, but in the case of the reinforced inomer, Su/ePLA/Su, there is a stabilization of CoF after 100 m of sliding distance. The highest friction takes place in the case of the unreinforced polymers, with values above 0.8 at the end of the tests, meanwhile in the case of the reinforced polymers the values are maintained below 0.5, indicating a higher wear performance of the PLA reinforced matrix.

Worn track observation using optical microscopy reveals the causes of the different CoF obtained (**Figure 11**). Pure Nucrel and Surlyn polymers present a worn track with plowing marks in the sliding direction of the steel counterbody. These marks reveal that the main wear mechanism for these specimens is abrasion, and this is the reason for the high CoF obtained. Debris produced by the abrasion of the tested material is usually attached to the counterbody, and the worn track itself is increasing its roughness due to the plowing marks due to the material removal. Both factors deal with the increase in the CoF as the sliding distance over the surface of the unreinforced specimen increases during the whole test (**Figure 10B**).

In the case of the reinforced polymers (**Figures 11C,D**), a change in the wear mechanism was observed. Nu/ePLA/Nu specimen shows a decrease in the abrasion (**Figure 11C**), with plowing marks only localized in the lateral zone of the worn track; but the central part of the track without evident signs of abrasion. Meanwhile, the Su/ePLA/Su ionomer sandwich-type structure composite (**Figure 11D**) shows a clear different worn track after the tribological tests. There is no evidence of abrasion, with a total absence of plowing marks in the sliding direction (arrow marked in **Figure 11D**), but some marks in the track perpendicular to the sliding direction are observed. The observation of the worn track at higher magnifications using 3D optical profilometer (**Figure 11E**) reveals the morphology of the worn track. The marks on the track are micro-plastic deformation of the material, revealing that this is the main wear mechanism of the PLA reinforced ionomer composite. This material has the ability to repair the mechanical damages at low

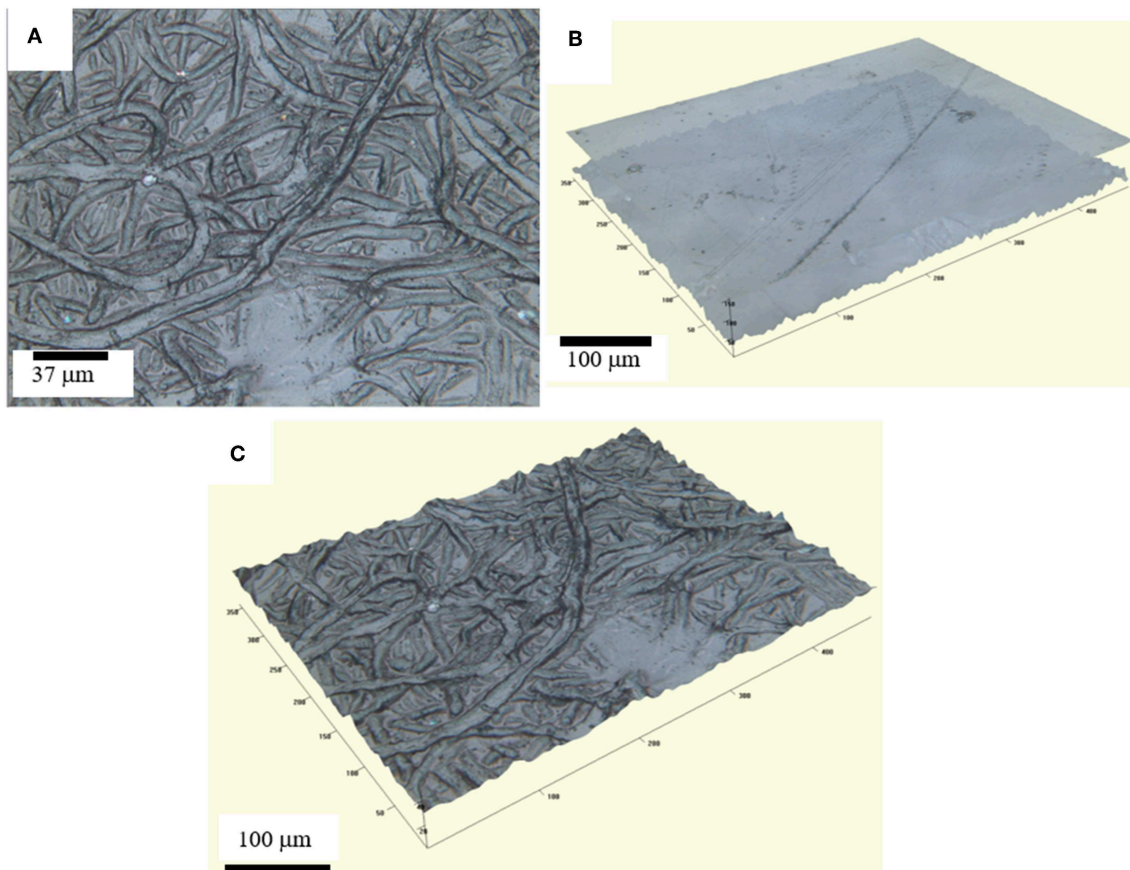


FIGURE 9 | 3D micrographs of the Su/ePLA/Su reinforced sandwich obtained with 3D Optical Profilometry: **(A)** plain view; **(B)** 3D micrograph with observation of the Surlyn® superior layer and the inner PLA layer; **(C)** 3D micrograph of the PLA inner layer.

temperature (above 40°C) when the own damage mechanism creates the enough temperature in the material, i.e., by friction between the damage object and the material, or an external heat source is applied to the material (López et al., 2018).

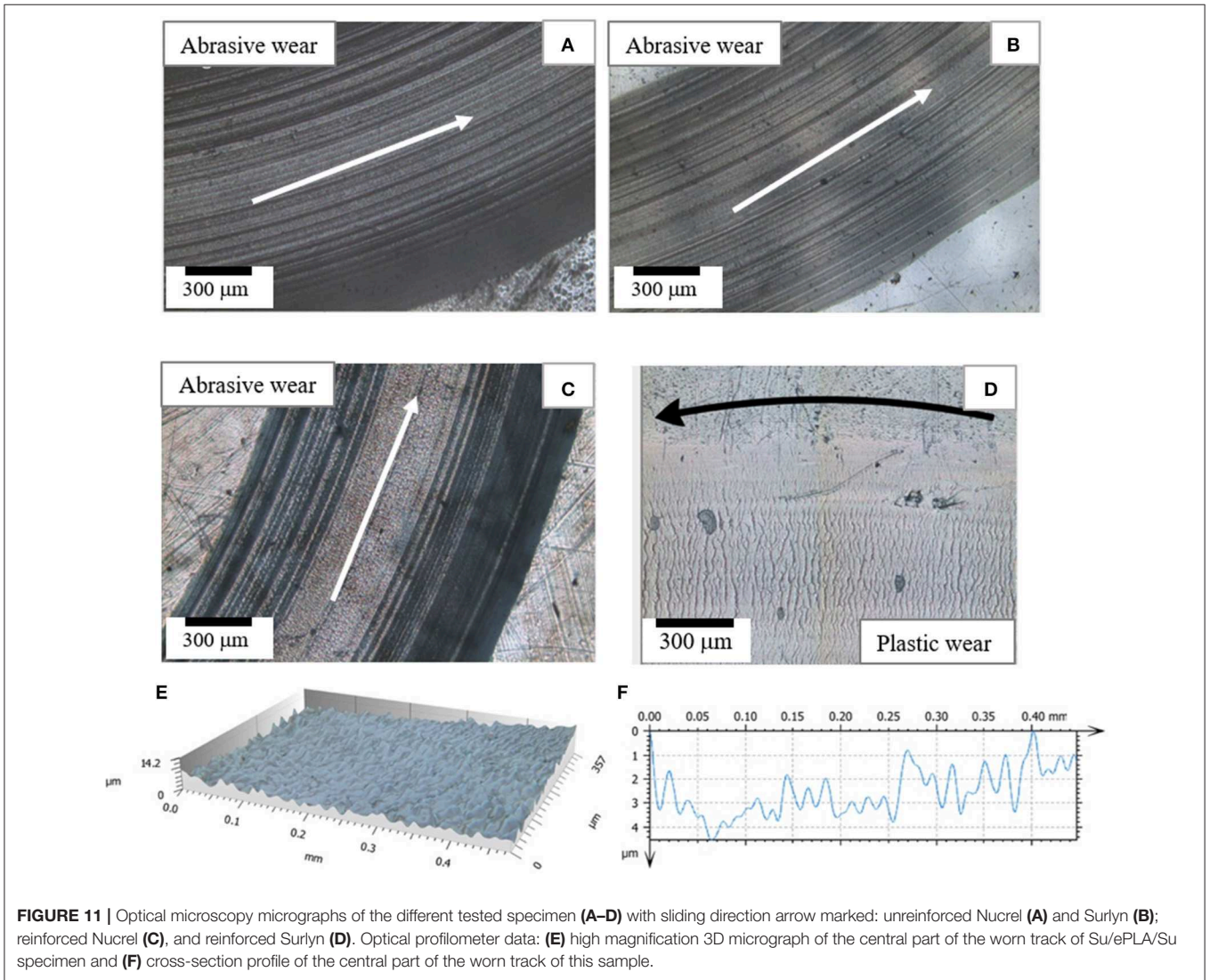
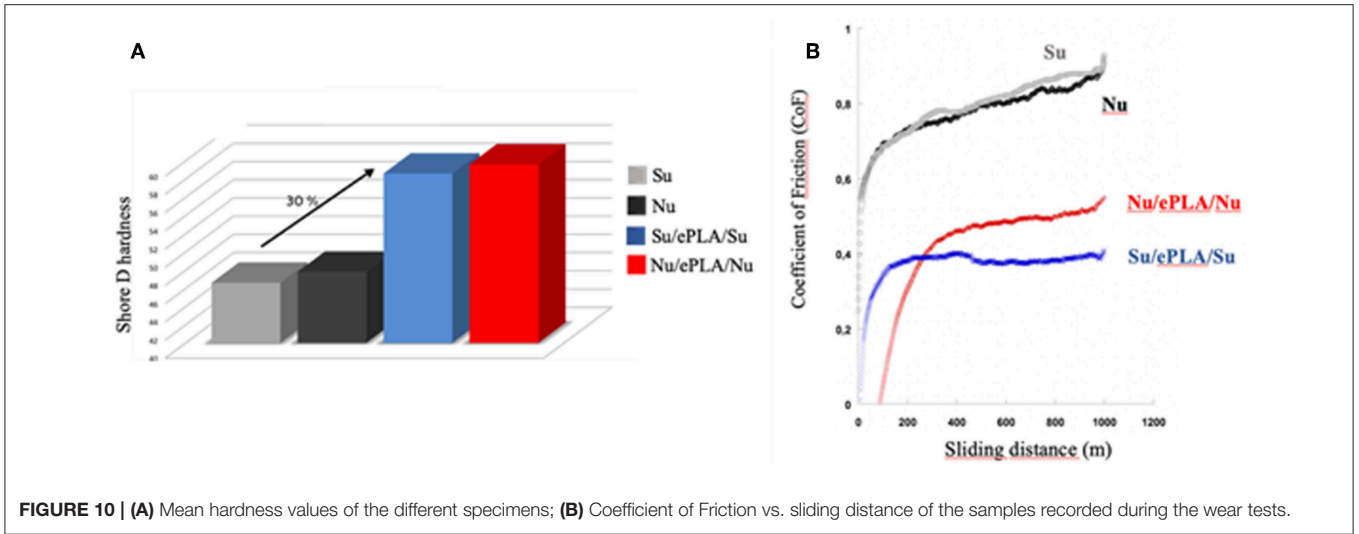
Table 3 collects some of the main morphological aspects of the worn tracks obtained after the wear tests. Roughness of the tracks was measured using 3D Optical Profilometry. Quadratic Surface Roughness (Sq) is used as a representative roughness value of the surface of the worn track of the specimens tested on its central zone.

It is clear that the abrasive mechanism creates a high roughness in the worn track, due to the detaching of material creating plowing marks, with Sq values between 2.1 and 3.8 μm . Meanwhile, in the case of the Su/ePLA7Su specimen, the Sq value decreases to 0.7 μm . The worn track of this specimen is smooth, with micro-plastic deformations in the track and absence of abrasion lines (**Figures 11D–F**). Furthermore, the worn depths calculated with the 3D Optical Profilometer of the different samples (**Figure 12**) reveal the different response to the wear test. Depth of the worn track is maximum in the case of the Nucler copolymer, with a value of 70 μm , as calculated using the 3D Optical Profilometry and the data analysis using

Mountain Map software (**Figure 12A**). The 3D reconstruction of the micrographs obtained, shown in **Figure 12** for the case of Nucler and Su/ePLA/Su, as representative responses, allows the calculation of the volume of the worn track using the Mountain software and with the use of the Equation (2), the Specific wear rate (k_v) can be determined, with a value of $2.8 \cdot 10^{-3}$ ($\text{mm}^3/\text{N m}$) for this sample.

The superior wear performance of the ionomer polymer Surlyn is clear, with a decrease of about 34 % in the worn track depth and of 46.4 % regarding to that of the Nucler copolymer.

Addition of PLA electrospun fibers in the polymer matrix has beneficial effects in the case of both Nucler and Surlyn matrix, mainly by the increase in the final material hardness, as reported in **Figure 10**. But the specific wear rate in the case of Su/ePLA/Su is two orders of magnitude lower than in the case of the unreinforced polymer, and this improvement is not obtained in the case of reinforced Nucler. Therefore, the change in the wear mechanism from abrasion to micro-plastic deformation has a beneficial effect in terms of wear performance and may be associated in some way to the self-healing ability of the ionomer. When observing a 3D micrograph of them, worn tracks in the case of Surlyn, the worn track depth is 41.5 μm in the



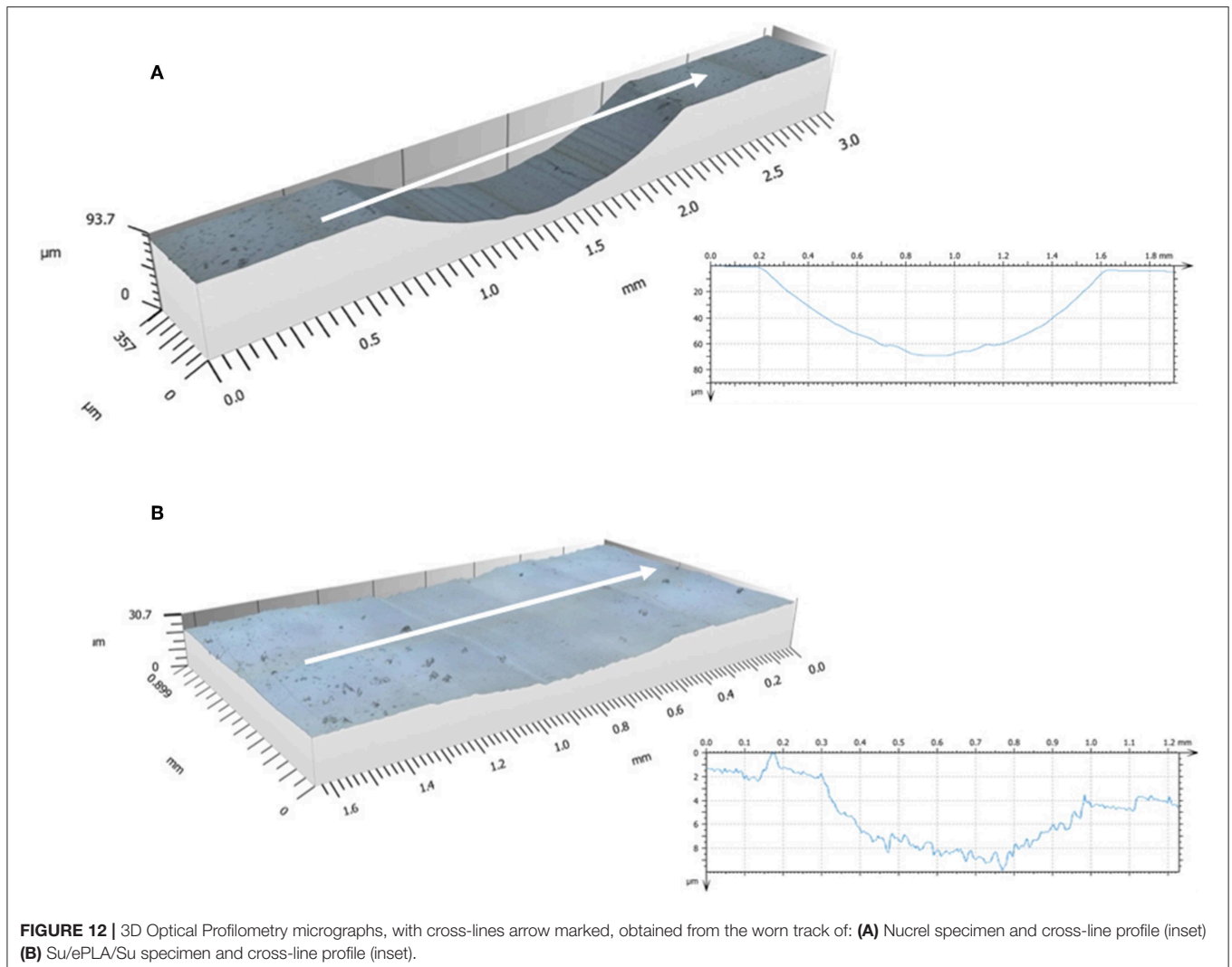
unreinforced material and just of $7.6\mu\text{m}$ in the case of the reinforced sample (**Figure 12B**). The depth of this worn track is very low, and this reflect the high response against wear of this Su/ePLA/Su composite with the lowest Specific wear rate of the studied materials in this work, $2.1 \times 10^{-5} \text{ mm}^3/\text{N m}$. This material has the ability to micro-deform plastically and in this way dissipates the energy of the wear process, without losing material due to abrasion, and without creating a hole as in the case of the rest of the tested materials (**Figures 11, 12A**).

TABLE 3 | Surface roughness, worn depth and Specific wear rate of the worn tracks of the different specimens.

Sample	Quadratic surface roughness S_q (μm)	Worn track depth (μm)	Specific wear rate k_v ($\text{mm}^3/\text{N m}$)
Nu	2.5	70.0	2.8×10^{-3}
Su	2.1	46.1	1.5×10^{-3}
Nu/ePLA/Nu	3.8	41.5	1.3×10^{-3}
Su/ePLA/Su	0.7	7.6	2.1×10^{-5}

CONCLUSIONS

Sandwich-type composites have been successfully obtained by adding electrospun microfibers to reinforce self-healing ionic polymers. In particular, three-layer stack based on PLA electrospun fibers in between two layers of commercial poly(ethylene-*co*-methacrylic acid) (EMAA) copolymers, well-know with the tradename of Nucrel[®] and Surlyn[®], both of them manufactured by Dupont[™] Company have been processed. Surlyn[®] is the corresponding ionomer of Nucrel[®] in which the MAA groups are partially neutralized with sodium ions. In these composites we solve the impregnation problem typically of composite materials. Therefore, in order to create the sandwich-type structure, firstly, the optimization of the processing window has achieved in order to maintain the randomly oriented fiber structure on the final composites. In particular, the creation of sandwich-type structure with Surlyn[®] reinforced with woven non-woven electrospun fibers based on PLA present enhanced mechanical response as well as hardness and wear resistance are improved. In particular, abrasion is the main wear mechanism



in all of the specimens with the exception of Su/ePLA/Su sample in which there is a change of behavior, with microplastic deformation as the main wear mechanism. Furthermore, wear resistance of Su/ePLA/Su specimen is two orders of magnitude higher than the rest of the materials tested, as a result of the specific wear rate obtained. Therefore, processing of sandwich-type composites reinforced with electrospun fibers can be considered as promising processing for future active packaging solutions.

DATA AVAILABILITY STATEMENT

All datasets generated for this study are included in the article/supplementary material.

AUTHOR CONTRIBUTIONS

VS performed the experimental analysis as well as the processing of the composite materials. AJL performed the hardness and wear analysis, as well as discussed the results. AL performs the electrospinning process and the characterization of the

materials. AU discussed the results. LP planned the work and helped in the experimental analysis and discussion of the results. All authors wrote and discussed the final version of the article.

FUNDING

MAT2017-88123-P, PCIN-2017-036, RYC-2014-15595, from MINEICO cofinanced with FEDER and AEI funds. S2018/NMT-4411 ADITIMAT-CM project, from Comunidad de Madrid.

ACKNOWLEDGMENTS

Authors thank the Spanish Ministry of Economy, Industry and Competitiveness (MINEICO) (MAT2017-88123-P, PCIN-2017-036) cofinanced with FEDER and AEI funds. Authors acknowledge the financial support received from Comunidad de Madrid (Additive Manufacturing from material to application Aditimat-CM project, S2018/NMT-4411) and Dupont™ Company for kindly providing the polymers. LP acknowledges the Ramon y Cajal (RYC-2014-15595) contract from MINEICO.

REFERENCES

- Amiraliyan, N., Nouri, M., and Kish, M. H. (2009). Effects of some electrospinning parameters on morphology of natural silk-based nanofibers. *J. Appl. Polym. Sci.* 113, 226–234. doi: 10.1002/app.29808
- Archard, J. F. (1953). Contact and rubbing of flat surfaces. *J. Appl. Phys.* 24, 981–988. doi: 10.1063/1.1721448
- Arrieta, M. P., López, J., López, D., Kenny, J. M., and Peponi, L. (2015). Development of flexible materials based on plasticized electrospun PLA-PHB blends: structural, thermal, mechanical and disintegration properties. *Eur. Polym. J.* 73, 433–446. doi: 10.1016/j.eurpolymj.2015.10.036
- Arrieta, M. P., López, J., López, D., Kenny, J. M., and Peponi, L. (2016a). Biodegradable electrospun bionanocomposite fibers based on plasticized PLA-PHB blends reinforced with cellulose nanocrystals. *Ind. Crops Prod.* 93, 290–301. doi: 10.1016/j.indcrop.2015.12.058
- Arrieta, M. P., López, J., López, D., Kenny, J. M., and Peponi, L. (2016b). Effect of chitosan and catechin addition on the structural, thermal, mechanical and disintegration properties of plasticized electrospun PLA-PHB biocomposites. *Polym. Degrad. Stab.* 132, 145–156. doi: 10.1016/j.polymdegradstab.2016.02.027
- Arrieta, P. M., Diez García, A., López, D., Fiori, S., and Peponi, L. (2019). Antioxidant bilayers based on PHBV and plasticized electrospun PLA-PHB fibers encapsulating catechin. *Nanomaterials* 9:346. doi: 10.3390/nano9030346
- ASTM (2015). *Standard Test Method for Rubber Property—Durometer Hardness*. West Conshohocken, PA: ASTM International.
- Barile, C., and Casavola, C. (2019). Mechanical characterization of carbon fiber reinforced plastics specimens for aerospace applications. *Polym. Compos.* 40, 716–722. doi: 10.1002/pc.24723
- Cai, S., Li, Y., Liu, H.-Y., and Mai, Y.-W. (2019). Effect of electrospun polysulfone/cellulose nanocrystals interleaves on the interlaminar fracture toughness of carbon fiber/epoxy composites. *Compos. Sci. Technol.* 181:107673. doi: 10.1016/j.compscitech.2019.05.030
- Calderón-Villajos, R., López, A. J., Peponi, L., Manzano-Santamaría, J., and Ureña, A. (2019). 3D-printed self-healing composite polymer reinforced with carbon nanotubes. *Mater. Lett.* 249, 91–94. doi: 10.1016/j.matlet.2019.04.069
- Carrasco-Hernandez, S., Gutierrez, J., Peponi, L., and Tercjak, A. (2017). Optimization of the electrospinning processing-window to fabricate nanostructured PE-b-PEO and hybrid PE-b-PEO/EBBA fibers. *Polym. Eng. Sci.* 57, 1157–1167. doi: 10.1002/pen.24492
- Cherpinski, A., Torres-Giner, S., Cabedo, L., Méndez, J. A., and Lagaron, J. M. (2018). Multilayer structures based on annealed electrospun biopolymer coatings of interest in water and aroma barrier fiber-based food packaging applications. *J. Appl. Polym. Sci.* 135:45501. doi: 10.1002/app.45501
- Dell'Anna, R., Lionetto, F., Montagna, F., and Maffezzoli, A. (2018). Lay-up and consolidation of a composite pipe by *in situ* ultrasonic welding of a thermoplastic matrix composite tape. *Materials* 11:e786. doi: 10.3390/ma11050786
- DiPoto, J. P. (1996). *Heat Sealable, High Moisture Barrier Film and Method of Making Same*. U.S. Patent No. 5,558,930. Washington, DC: U.S. Patent and Trademark Office.
- Dolog, R., and Weiss, R. A. (2013). Shape memory behavior of a polyethylene-based carboxylate ionomer. *Macromolecules* 46, 7845–7852. doi: 10.1021/ma401631j
- Eisenberg, A., and Navratil, M. (1974). Ion clustering and viscoelastic relaxation in styrene-based ionomers. IX-Ray V. and dynamic mechanical studies. *Macromolecules* 7, 90–94. doi: 10.1021/ma60037a018
- Fang, J., Niu, H., Lin, T., and Wang, X. (2008). Applications of electrospun nanofibers. *Chin. Sci. Bull.* 53, 2265–2286. doi: 10.1007/s11434-008-0319-0
- Francesconi, A., Giacomuzzo, C., Grande, A. M., Mudric, T., Zaccariotto, M., Etemadi, E., et al. (2013). Comparison of self-healing ionomer to aluminium-alloy bumpers for protecting spacecraft equipment from space debris impacts. *Adv. Space Res.* 51, 930–940. doi: 10.1016/j.asr.2012.10.013
- Jantanasakulwong, K., Kobayashi, Y., Kuboyama, K., and Ougizawa, T. (2016). Thermoplastic vulcanizate based on Poly(lactic acid) and acrylic rubber blended with ethylene ionomer. *J. Macromol. Sci. Part B* 55, 1068–1085. doi: 10.1080/00222348.2016.1238434
- Kalista, S. J. Jr., and Ward, S. J. (2007). Thermal characteristics of the self-healing response in poly(ethylene-co-methacrylic acid) copolymers. *J. Roy. Soc. Int.* 4, 405–411. doi: 10.1098/rsif.2006.0169
- Kar, K. K. (2016). *Composite Materials: Processing, Applications, Characterizations*. Berlin; Heidelberg: Springer.
- Khalid, M. A. U., Ali, M., Soomro, A. M., Kim, S. W., Kim, H. B., Lee, B.-G., et al. (2019). A highly sensitive biodegradable pressure sensor based on nanofibrous dielectric. *Sens. Actuat. A Phys.* 294, 140–147. doi: 10.1016/j.sna.2019.05.021
- Kim, T.-E., Bae, J. C., Cho, K. Y., Shul, Y.-G., and Kim, C. Y. (2013). Fabrication of electrospun SiC fibers web/phenol resin composites for the application to high thermal conducting substrate. *J. Nanosci. Nanotechnol.* 13, 3307–3312. doi: 10.1166/jnn.2013.7264

- Kim, W. J., and Lee, S. J. (2016). The effect of the melt viscosity and impregnation of a film on the mechanical properties of thermoplastic composites. *Materials* 9:E448. doi: 10.3390/ma9060448
- Kimna, C., Tamburaci, S., and Tihminlioglu, F. (2019). Novel zein-based multilayer wound dressing membranes with controlled release of gentamicin. *J. Biomed. Mater. Res. Part B Appl. Biomater.* 107, 2057–2070. doi: 10.1002/jbm.b.34298
- Krabbenborg, F. J. T., Mangnus, M. A., Belot, P. C., and Leon, J. (2007). *Reactive Hot Melt Adhesive*. U.S. Patent No. 7,271,202. Washington, DC: U.S. Patent and Trademark Office.
- Ku, H., Wang, H., Pattarachaiyakoo, N., and Trada, M. (2011). A review on the tensile properties of natural fiber reinforced polymer composites. *Composit. Part B Eng.* 42, 856–873. doi: 10.1016/j.compositesb.2011.01.010
- Kuwabara, K., and Horii, F. (2002). Solid-state NMR analyses of the crystalline–noncrystalline structure and its thermal changes for ethylene ionomers. *J. Polymer Sci. Part B Polymer Phys.* 40, 1142–1153. doi: 10.1002/polb.10174
- Lamastra, F. R., Puglia, D., Monti, M., Vella, A., Peponi, L., Kenny, J. M., et al. (2012). Poly(ϵ -caprolactone) reinforced with fibres of Poly(methyl methacrylate) loaded with multiwall carbon nanotubes or graphene nanoplatelets. *Chem. Eng. J.* 195–196, 140–148. doi: 10.1016/j.cej.2012.04.078
- Leonés, A., Sonseca, A., López, D., Fiori, S., and Peponi, L. (2019). Shape memory effect on electrospun PLA-based fibers tailoring their thermal response. *Eur. Polym. J.* 117, 217–226. doi: 10.1016/j.eurpolymj.2019.05.014
- Lertngim, A., Phiriyawirut, M., Woothikanokkan, J., Yuwawech, K., et al. (2017). Preparation of Surlyn films reinforced with cellulose nanofibres and feasibility of applying transparent composite films for organic photovoltaic encapsulation. *Roy. Soc. Open Sci.* 4, 1–18. doi: 10.1098/rsos.170792
- Li, D., and Xia, Y. (2004). Electrospinning of nanofibers: reinventing the wheel? *Adv. Mater.* 16, 1151–1170. doi: 10.1002/adma.200400719
- Loo, Y.-L., Wakabayashi, K., Huang, Y. E., Register, R. A., and Hsiao, B. S. (2005). Thin crystal melting produces the low-temperature endotherm in ethylene/methacrylic acid ionomers. *Polymer* 46, 5118–5124. doi: 10.1016/j.polymer.2005.04.043
- López, A. J., Teno, J., Ureña, A., and Rams, J. (2018). “Healing ability of ionomeric polymers under low-energy transfer damages,” in *How Smart Are the Polymers*, ed. J. M. R. E. Laura Peponi (New York, NY: Nova Science Publishers), 149–174.
- López-Córdoba, A., Estevez-Areco, S., and Goyanes, S. (2019). Potato starch-based biocomposites with enhanced thermal, mechanical and barrier properties comprising water-resistant electrospun poly (vinyl alcohol) fibers and yerba mate extract. *Carbohydr. Polym.* 215, 377–387. doi: 10.1016/j.carbpol.2019.03.105
- Lu, L., and Li, G. (2016). One-way multishape-memory effect and tunable two-way shape memory effect of ionomer Poly(ethylene-co-methacrylic acid). *ACS Appl. Mater. Interfaces* 8, 14812–14823. doi: 10.1021/acsami.6b04105
- Marx, C. L., and Cooper, S. L. (1974). The crystallinity of ionomers. *J. Macromol. Sci. Part B* 9, 19–33. doi: 10.1080/00222347408204538
- Mujica-García, A., Navarro-Baena, I., Kenny, J. M., and Peponi, L. (2014). Influence of the processing parameters on the electrospinning of biopolymeric fibers. *J. Renew. Mater.* 2, 23–34. doi: 10.7569/JRM.2013.634130
- Oroujzadeh, M., Etesami, M., and Mehdipour-Ataei, S. (2019). Poly(ether ketone) composite membranes by electrospinning for fuel cell applications. *J. Power Sources* 434:226733. doi: 10.1016/j.jpowsour.2019.226733
- Peponi, L., Puglia, D., Torre, L., Valentini, L., and Kenny, J. M. (2014). Processing of nanostructured polymers and advanced polymeric based nanocomposites. *Mater. Sci. Eng. R Rep.* 85, 1–46. doi: 10.1016/j.mser.2014.08.002
- Persano, L., Camposeo, A., Tekmen, C., and Pisignano, D. (2013). Industrial upscaling of electrospinning and applications of polymer nanofibers: a review. *Macromol. Mater. Eng.* 298, 504–520. doi: 10.1002/mame.201200290
- Pickering, K. L., Efendy, M. G. A., and Le, T. M. (2016). A review of recent developments in natural fibre composites and their mechanical performance. *Composit. Part A Appl. Sci. Manufact.* 83, 98–112. doi: 10.1016/j.compositesa.2015.08.038
- Quiles-Carrillo, L., Montanes, N., Lagaron, M. J., Balart, R., and Torres-Giner, S. (2019). Bioactive multilayer polylactide films with controlled release capacity of gallic acid accomplished by incorporating electrospun nanostructured coatings and interlayers. *Appl. Sci.* 9:533. doi: 10.3390/app9030533
- Salomi, A., Greco, A., Felling, F., Manni, O., and Maffezzoli, A. (2007). A preliminary study on bladder-assisted rotomolding of thermoplastic polymer composites. *Adv. Polymer Technol.* 26, 21–32. doi: 10.1002/adv.20085
- Sessini, V., Brox, D., López, A. J., Ureña, A., and Peponi, L. (2018). Thermally activated shape memory behavior of copolymers based on ethylene reinforced with silica nanoparticles. *Nanocomposites* 4, 19–35. doi: 10.1080/20550324.2018.1472723
- Sessini, V., Raquez, J.-M., Kenny, J. M., Dubois, P., and Peponi, L. (2019). Melt-processing of bionanocomposites based on ethylene-co-vinyl acetate and starch nanocrystals. *Carbohydr. Polym.* 208, 382–390. doi: 10.1016/j.carbpol.2018.12.095
- Sonseca, A., Peponi, L., Sahuquillo, O., Kenny, J. M., and Giménez, E. (2012). Electrospinning of biodegradable polylactide/hydroxyapatite nanofibers: Study on the morphology, crystallinity structure and thermal stability. *Polym. Degrad. Stab.* 97, 2052–2059. doi: 10.1016/j.polymdegradstab.2012.05.009
- Sundaresan, V. B., Morgan, A., and Castellucci, M. (2013). Self-healing of ionomeric polymers with carbon fibers from medium-velocity impact and resistive heating. *Smart Mater. Res.* 2013:271546. doi: 10.1155/2013/271546
- Tachino, H., Hara, H., Hirasawa, E., Kutsumizu, S., Tadano, K., and Yano, S. (1993). Dynamic mechanical relaxations of ethylene ionomers. *Macromolecules* 26, 752–757. doi: 10.1021/ma00056a029
- Tsujita, Y., Shibayama, K., Takizawa, A., Kinoshita, T., and Uematsu, I. (1987). Thermal properties of ethylene ionomers. *J. Appl. Polym. Sci.* 33, 1307–1314. doi: 10.1002/app.1987.070330421
- Varley, R. (2007). Ionomers as self healing polymers. *Springer Ser. Mater. Sci.* 100, 95–114. doi: 10.1007/978-1-4020-6250-6_5
- Varley, R. J., Shen, S., and van der Zwaag, S. (2010). The effect of cluster plasticisation on the self healing behaviour of ionomers. *Polymer* 51, 679–686. doi: 10.1016/j.polymer.2009.12.025
- Varley, R. J., and van der Zwaag, S. (2008). Towards an understanding of thermally activated self-healing of an ionomer system during ballistic penetration. *Acta Mater.* 56, 5737–5750. doi: 10.1016/j.actamat.2008.08.008
- Vega, J. M., Grande, A. M., van der Zwaag, S., and García, S. J. (2014). On the role of free carboxylic groups and cluster conformation on the surface scratch healing behaviour of ionomers. *Eur. Polym. J.* 57, 121–126. doi: 10.1016/j.eurpolymj.2014.05.005
- Wang, X., Jiang, M., Zhou, Z., Gou, J., and Hui, D. (2017). 3D printing of polymer matrix composites: a review and prospective. *Composites Part B Eng.* 110, 442–458. doi: 10.1016/j.compositesb.2016.11.034
- Weigel, P. (1981). *Macromolecular physics*. Vol. 3: Crystal melting. Von BERNHARD WUNDERLICH. New York/London/Toronto/Sydney/San Francisco: Academic Press 1980. XIII, 363 S., Lwd., \$ 42.50. *Acta Polymerica* 32:413. doi: 10.1002/actp.1981.010320709
- Zhao, Z., Peng, F., Cavicchi, K. A., Cakmak, M., Weiss, R. A., and Vogt, B. D. (2017). Three-dimensional printed shape memory objects based on an olefin ionomer of Zinc-Neutralized Poly(ethylene-co-methacrylic acid). *ACS Appl. Mater. Interfaces* 9, 27239–27249. doi: 10.1021/acsami.7b07816
- Zhu, H., Wu, B., Li, D., Zhang, D., and Chen, Y. (2011). Influence of voids on the tensile performance of carbon/epoxy fabric laminates. *J. Mater. Sci. Technol.* 27, 69–73. doi: 10.1016/S1005-0302(11)60028-5

Conflict of Interest: The authors declare that the research was conducted in the absence of any commercial or financial relationships that could be construed as a potential conflict of interest.

Copyright © 2019 Sessini, López Galisteo, Leonés, Ureña and Peponi. This is an open-access article distributed under the terms of the Creative Commons Attribution License (CC BY). The use, distribution or reproduction in other forums is permitted, provided the original author(s) and the copyright owner(s) are credited and that the original publication in this journal is cited, in accordance with accepted academic practice. No use, distribution or reproduction is permitted which does not comply with these terms.